Structure-Dynamic Analysis of an Induction Machine with Eccentric Rotor Movement

C. Schlensok, D. van Riesen, and K. Hameyer

Abstract — **In recent years the analysis and estimation of noise and vibration have been gaining interest. Both, noise and vibration are often due to the electromagnetic forces in electric machinery such as induction machines with squirrel-cage rotors. Manufacturing tolerances and faults have great impact to the electromagnetic behaviour of electric machines. Therefore, many studies have been presented concerning the analysis of noise and vibration in electric machinery. Here, a major task, the eccentric rotor movement, is studied, applying the finite-element method and analytical models for the structure-dynamic analysis of an induction machine with squirrel cage rotor.**

Index Terms — **FEM, induction machine, acoustics, eccentric rotor movement, structure dynamics, vibrations.**

I. Introduction

MANY studies have been presented concerning the electromagnetic and structure dynamic behaviour of Induction Machines with squirrel-cage rotor (IM) with eccentric rotor movement [1-4]. The latter usually do not consider any simulation results which allow the de-coupling of the impact of eccentric rotor movement from other effects. This might be due to the high computational costs or a lack of software tools. Here, exactly this is presented applying the Finite-Element Method (FEM) and the analytic model of [1,2].

Eccentric rotor movement of electrical machines causes extra disturbing noise and vibrations. This extra noise can either occur in terms of additional electromagnetic force harmonics or in terms of an amplification of harmonics stemming from the fundamental or saturational fields. The detection of additional harmonics allows for a detailed analysis of the IM's acoustics in both analytical models and measurements [1,3,4]. The impact of the amplification is rather hard to estimate by measurement and analytic models. Especially in measurements it is nearly impossible to assure that the reference machine does not have any eccentricity. Therefore, the aspect of eccentric rotor movement is studied in detail in this paper by means of numeric simulation. Numeric models allow for the extraction of single effects and preparation of ideal reference models.

Next to centric there are two different types of eccentric rotor movements, as Fig. 1 resumes:

1. dynamic eccentricity and
2. static eccentricity.

In the centric case the rotor, stator, and rotational axis lie in the same location. For the case of dynamic eccentricity the rotor axis is shifted to one side. The rotational axis remains in the same location as the stator axis. This way the rotor performs a whiling motion. Finally, the static eccentricity results in the shifting of both rotor and rotational axis. The rotor keeps rotating stationary.

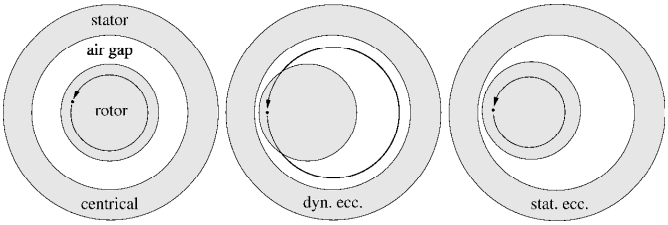

Fig. 1. Types of eccentric rotor movement.

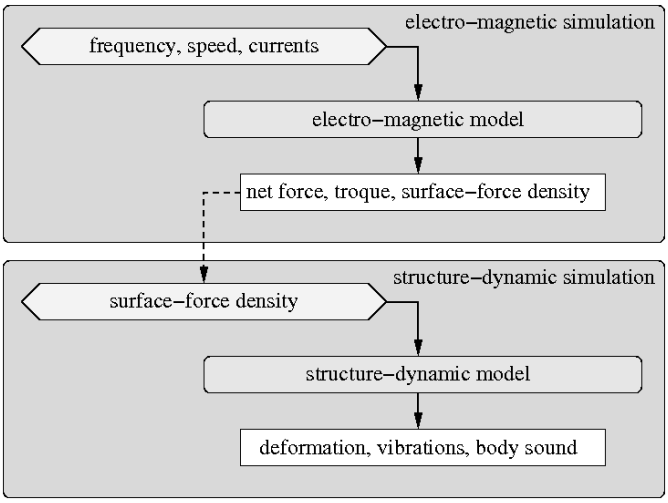

Fig. 2. Flow chart of the structure-dynamic simulation-chain.

Fig. 2 shows the flowchart of the entire structure-dynamic simulation chain. At first an electromagnetic model is prepared considering the non-linear behaviour of the iron laminations, the rotor movement, and the stator currents. Here, the models are adapted depending on the type of eccentricity simulated. Four different models are studied:

1. centric model without eccentricity,
2. dynamic eccentric model,
3. static eccentric model, and
4. a combined static-dynamic eccentric model with 50 % of each type of eccentricity.

The Finite-Element Method (FEM) [5,6] is applied for both the electromagnetic using the multi-slice method and the structure-dynamic simulation [9-11].

Manuscript received July 15th, 2006.

C. Schlensok, D. van Riesen, and K. Hameyer are with the Institute of Electrical Machines, RWTH Aachen University, D-52056 Aachen, Germany. (phone: +49-241-8097667; fax: +49-241-8092270; e-mail: Christoph.Schlensok@ iem.rwth-aachen.de).

II. Electromagnetic Simulation

The electromagnetic FE-models consist of stator and rotor including the 3-phase, 2-layer winding of the stator and the aluminium-cast rotor-bars. Between stator and rotor the air gap is located. This is modelled as well. The flux has to cross over. For numeric and modelling reasons (i.e. the rotational movement) a 3-layer air-gap is constructed. Fig. 6 shows a zoom of the air gap region with meshed air-gap layers. The central layer marked with l_C is used for re-meshing while applying the moving-band method [7]. The outer layer l_S is connected to the stator, and the inner layer l_R is fixed to the rotor and is rotated in every time step together with the rotor. Hence, dynamic eccentric rotor movement results in an eccentric rotor air-gap layer (Fig. 4) and the static eccentricity in an eccentric stator air-gap region (Fig. 5)). A combined eccentric model of course has both an eccentric stator and an eccentric rotor air-gap layer. For the centric reference model three concentric air-gap layers are modelled.

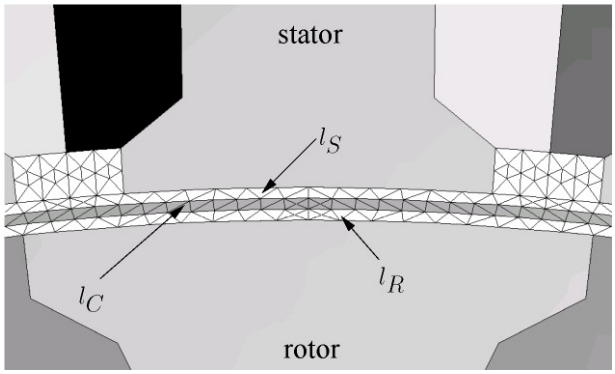

Fig. 3. Zoom of air-gap region of the centric electromagnetic FE-model.

The two types of eccentric rotor movement are described in The electromagnetic simulation provides the magnetic flux-density distribution for each of the $N = 4200$ performed simulation- time steps. With this the torque T, net force F, and the surface-force density σ are calculated. The analysis of T, F, and σ in the case of eccentric rotor movement is described in [8]. The torque hardly shows any impact by the eccentricity. Nevertheless, the net force is affected seriously. Eccentricity results in very high net-force magnitudes acting onto the bearings. For the studied IM the maximum forces reached for dynamic eccentricity exceed the mechanical forces of an unbalanced rotor at the same rotor speed by far.

The time-dependent behaviour of the surface-force density for a single element on the up-running edge of a stator tooth is shown in Fig. 6. The force pulsates depending on the speed n, the number of rotor slots N_R, the stator frequency f_1, and the number of pole pairs p.

For the structure-dynamic analysis σ is transformed into the frequency domain (Fig. 7). With the resulting spectrum and the analytic model of [1] a set of frequencies is selected. All of them are not special to the effect of eccentricity, since the amplification effect of the harmonics is studied explicitly, here. Additional frequencies resulting from eccentricity are not studied in the first step. Table I lists the selected frequencies.

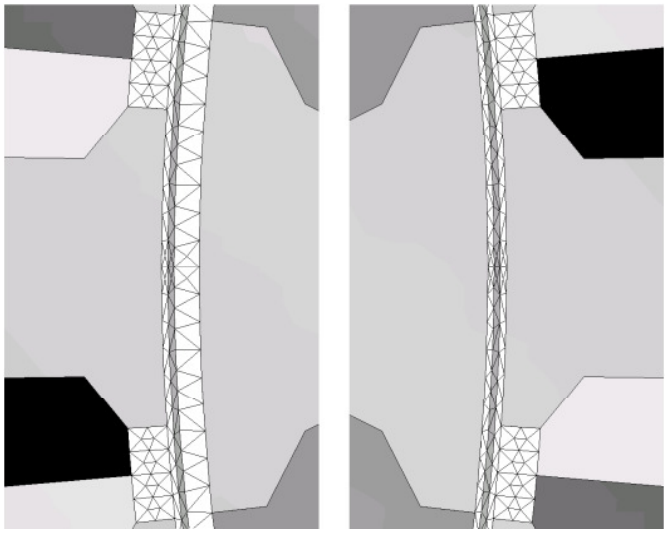

Fig. 4. Zoom of air-gap region of dynamic eccentric FE-model.

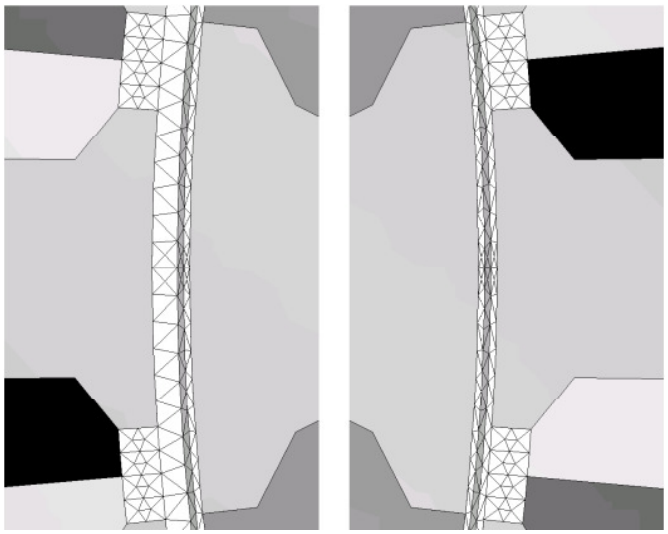

Fig. 5. Zoom of air-gap region of static eccentric FE-model.

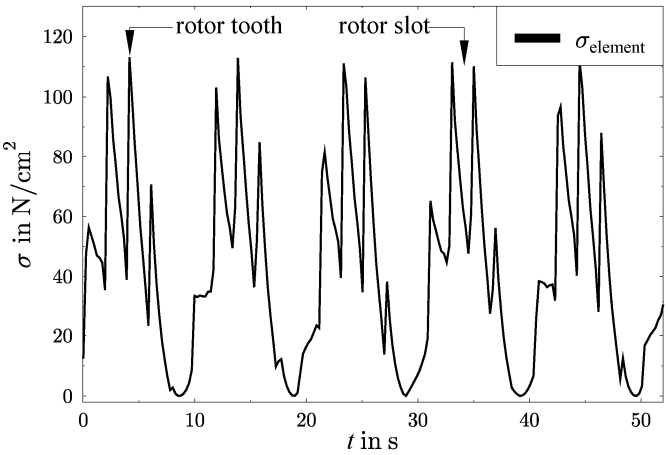

Fig. 6. Time-dependent behavior of the surface-force density.

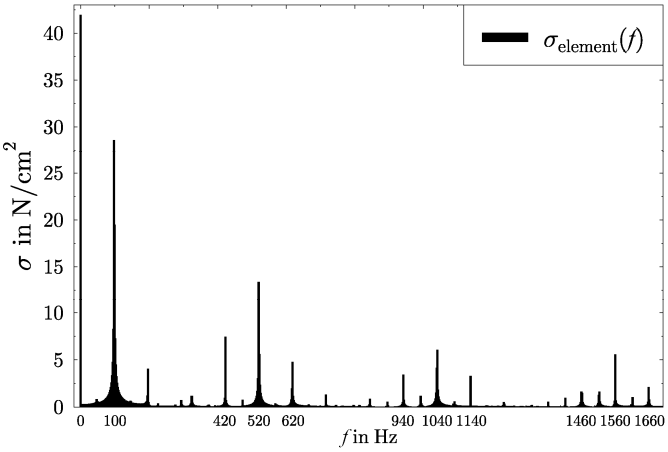

Fig. 6. Spectrum of the surface-force density.

Table. I. Selected frequencies from the surface-force density-spectrum.

f [Hz]	98	422	520	618
f [Hz]	716	942	1040	1138

III. Structure-dynamic Simulation

The structure-dynamic simulation is performed for all four different force excitations resulting from the electromagnetic models. The mechanical simulation provides the deformation for all nodes of the structure-dynamic model. The structure-dynamic FE-model depicted in Fig. 7 consists of all mechanical parts such as stator with winding, rotor with short-circuit rings, shaft, bearings, end shields with rubber rings, and the housing which is coupled to the stator with six spiral-steel springs. The surface-force density of each of the four electromagnetic models is transformed to the stator teeth of the mechanical model in the frequency domain for the set of selected frequencies.

The deformation is simulated with linear material behaviour. Therefore, complex values can be applied. An example for the deformation of the IM is shown in Fig. 8. Here, the deformation of housing and stator is depicted for one single point in time. As can be seen the magnitudes of the nodal oscillations of the stator is significantly higher than for the housing. This is due to the coupling of stator and housing by spiral-steel springs reducing the transmitted vibrations.

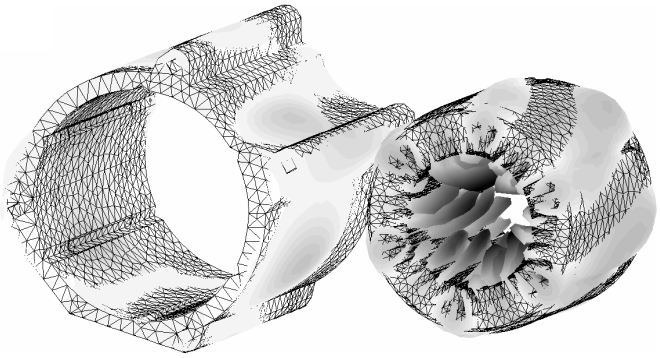

Fig. 8. Example for the deformation of housing and stator at f = 618 Hz.

Since the application of the IM is not in direct influence range of the human ear, it is of higher interest to study the body sound which can be transmitted and then be decoupled as acoustic noise in hearing range [12]. Therefore, the deformation of the IM is analyzed by three different criteria:

1. the deviation of the deformation between an eccentric model and the centric reference model,
2. the body-sound level L_S along the circumference of the housing along two lines on both ends of the IM, and
3. the body-sound index L_{BSI} of the housing allowing for the absolute comparison of the deformation.

Next to these criteria the deformation can be analyzed by means of the oscillation modes r [1,2]. In the following the results are discussed in detail.

A. *Modes of oscillation*

The oscillation modes detected in the simulation model match the predicted modes from the analytical model of [1]. Fig. 9 shows exemplarily two modes of oscillation which are due to eccentricity concerning the studied IM. The regarded frequency is f = 20 Hz which is the rotor speed. For this fre-

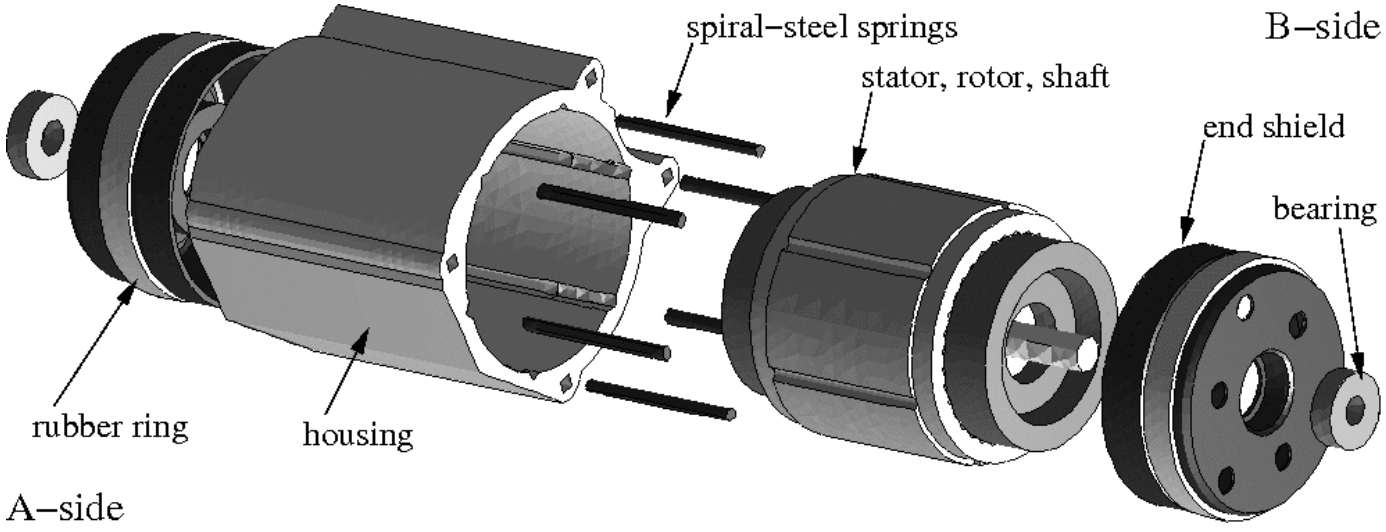

Fig. 7. Structure-dynamic FE-model of the induction machine with squirrel-cage rotor.

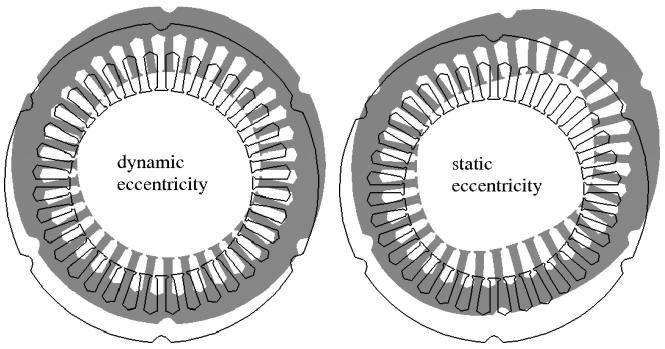

Fig. 9. Example for oscillation modes at $f = 20$ Hz.

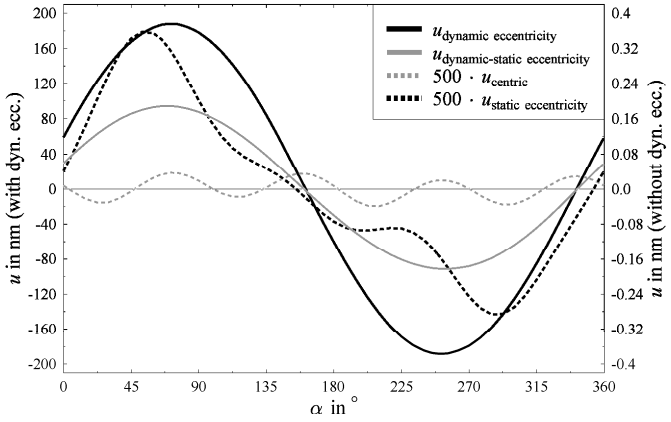

Fig. 10. Deformation along outer circumference of stator at $f = 20$ Hz.

quency the dynamic eccentricity shows the highest impact. Without any eccentricity there is a very low and insignificant deformation stated. The static eccentric case shows a slightly higher deformation with mode number $r = 4$. For the dynamic eccentric case the revolving force wave results in an oscillation mode r = 1 with a very high magnitude. The exaggerated deformation in Fig. 9 is 500 times as high for the dynamic case when compared to the static. This is resumed by Fig. 10. The deformation is sampled along the outer circumference of the stator.

B. Deviation of the deformation

In a second step the deviation of the deformation is analyzed. The deviation is calculated by subtracting the results of the deformation of the reference model (centric electromagnetic model) from each of the three eccentric models. By this, it is possible to detected regions for example of the housing which are deformed stronger by eccentric rotor movement.

Fig. 11 exemplarily shows the deviation of the deformation at $f = 422$ Hz for the three cases. For the dynamic eccentric case it can be seen the deviation is positive in general. The dynamic eccentricity results in higher deformation of the stator and housing for this frequency. The studies have shown that this is the fact for all selected frequencies. As the plots of the static and combined eccentric models show static eccentricity results in a significant increase of the deformation for most of the housing. Except for the white region opposite of the location of the smallest air-gap width the deformation is by far

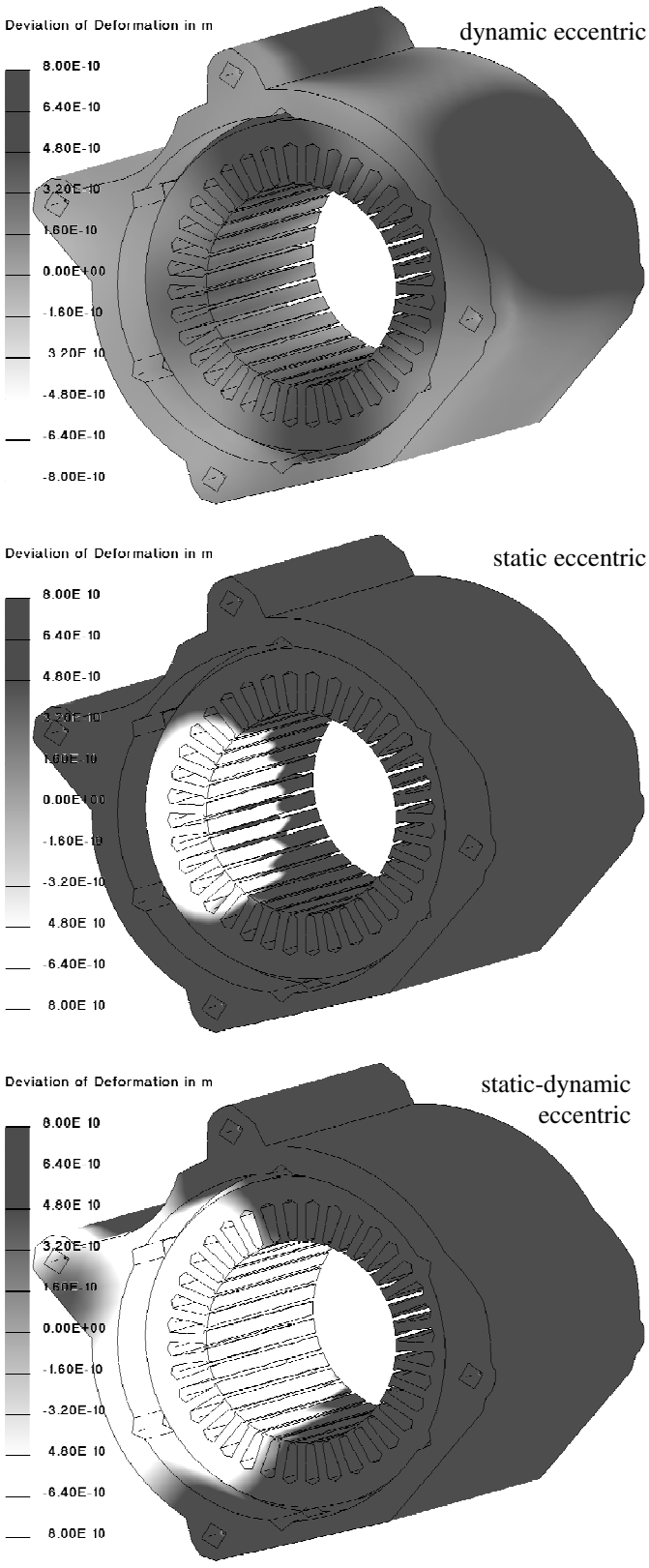

Fig. 11. Deviation of deformation of housing at $f = 422$ Hz.

higher than in the case of a centric or dynamic eccentric rotor movement.

Next to this, the vibrations of the IM depend in the case of static eccentricity strongly on the location of the smallest air

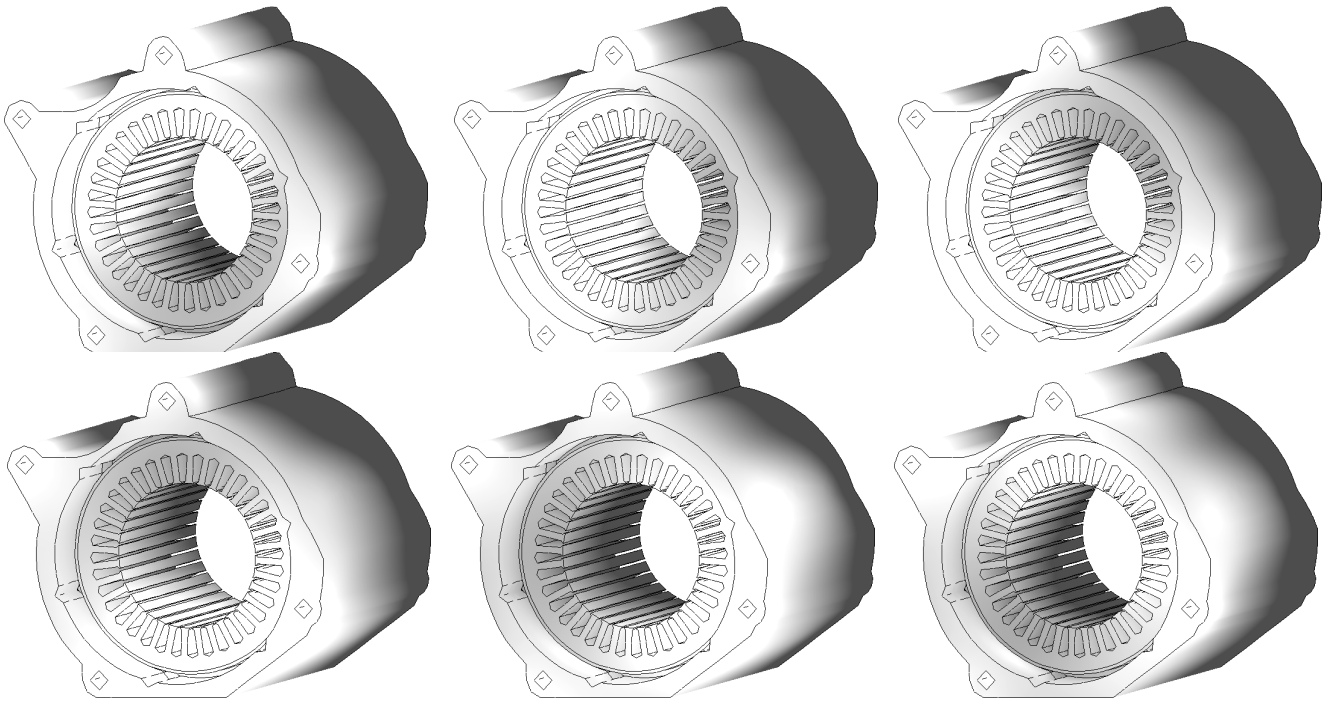

Fig. 12. Deviation of Deformation for four different location of the static eccentricity at f = 422 Hz.

gap. This is due to the asymmetric construction of the housing. Fig. 12 shows six models with static eccentricity. In each model the location of the smallest air gap is rotated 60° clockwise. The highest deviation is found on the back side (B-side) of the IM. This is due to the mounting of the IM on the surface plate of the housing on the A-side. Here, the IM is fixed with four screws which do not allow high deformation. The deviation of the deformation varies significantly when looking at the same spot, e.g. on the outer surface of the housing. Therefore, it is not possible to detect a static eccentric IM by measuring the body-sound level on one spot of the housing. It is necessary to at least place two sensors positioned in a 90° angle. Otherwise, a static eccentric IM might occur to be very good, i.e. having a low body sound, instead of being rejected.

C. Body-sound level

The second analysis criterion is the body-sound level L_S. The deformation in a single location on the surface of the housing is sampled and transformed into the complex-valued acceleration $\underline{a}$ in local cylinder coordinates and depending on the studied frequency $\omega = 2\pi f$:

$$\vec{\underline{a}} = -\omega^2 \cdot \vec{\underline{u}}_{\text{local}} \ . \tag{1}$$

The local coordinates depend on the location of the sampling point on the housing:

$$\vec{\underline{u}}_{local} = \begin{pmatrix} \underline{x} \cdot \vec{e}_x \cdot \vec{e}_{rad} + \underline{y} \cdot \vec{e}_y \cdot \vec{e}_{rad} + \underline{z} \cdot \vec{e}_z \cdot \vec{e}_{rad} \\ \underline{x} \cdot \vec{e}_x \cdot \vec{e}_{\tan} + \underline{y} \cdot \vec{e}_y \cdot \vec{e}_{\tan} + \underline{z} \cdot \vec{e}_z \cdot \vec{e}_{\tan} \\ \underline{x} \cdot \vec{e}_x \cdot \vec{e}_{ax} + \underline{y} \cdot \vec{e}_y \cdot \vec{e}_{ax} + \underline{z} \cdot \vec{e}_z \cdot \vec{e}_{ax} \end{pmatrix} . \tag{2}$$

With this L_S is calculated by

$$L_S = 20 \cdot \log \frac{|\underline{a}|}{a_{ref}} \text{dB} \ . \tag{3}$$

Where a_{ref} = 1 µm/s^2 is a reference value. L_S is calculated along two circumferential lines on both ends of the housing's surface as Fig. 13 shows.

The analysis of the radial component of L_S on both ends of the housing is shown in Fig. 14 for the A-side and in Fig. 15 for the B-side for f = 422 Hz. On the A-side L_S varies strongly depending on the location. There are four local minima which stem from the mounting with four screws. The six maxima result from the six spiral-steel springs. At their location the deformation of the stator is transmitted to the housing. The

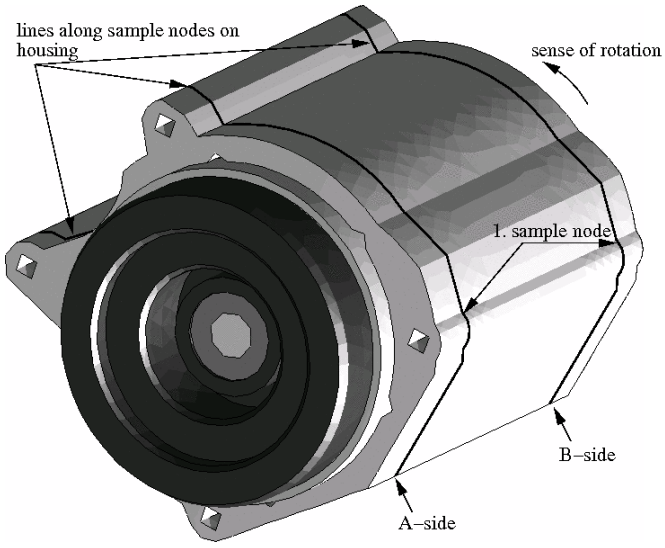

Fig. 13. Sampling lines for the calculation of the body-sound level L_S.

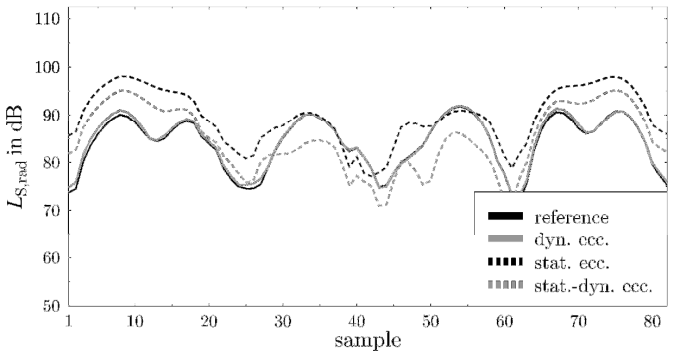

Fig. 14. Body-sound level L_S on A-side of housing at f = 422 Hz.

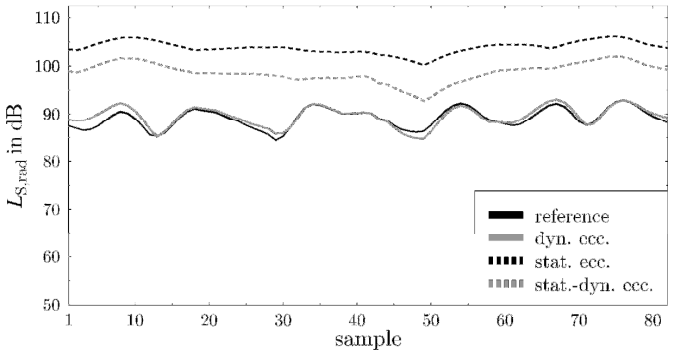

Fig. 15. Body-sound level L_S on B-side of housing at f = 422 Hz.

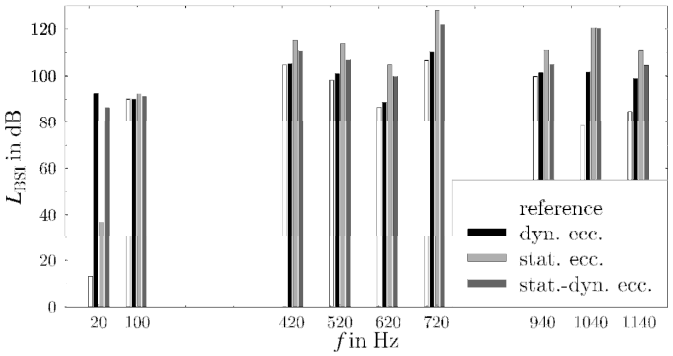

Fig. 16. Body-sound index L_{BSI} of the housing.

centric and dynamic eccentric model result in nearly the same body-sound level for this frequency. Static eccentricity reaches the highest values. The combination of both types of eccentricity lies in-between. The position of the smallest and the largest air gap can be located in the case of static eccentric rotor movement, coinciding with the highest and the lowest values of L_S.

D. Body-sound index

Finally the body-sound index L_{BSI} representing the entire deformation of a body, e.g. the housing, is calculated and analysed. In the case of dynamic eccentricity the L_{BSI} increases slightly with the exception of rotor speed f = 20 Hz and the two highest studied frequencies f = 1040 and 1138 Hz. Here, L_{BSI} raises significantly. Except for rotor speed static eccentric rotor movement results in the highest peaks throughout the spectrum reaching the highest overall value at the first stator-slot harmonic at f = 720 Hz. The combined eccentric model shows the high impact of the static eccentricity. Here, the values are increased very strongly as well.

IV. Conclusions

The paper presents the structure-dynamic analysis of an induction machine with squirrel-cage rotor (IM) with eccentric rotor movement. The different types of eccentricity are introduced and their consideration in the electromagnetic Finite-Element (FE)-models is described. The results of the electromagnetic simulation are discussed focussing on the surface-force density excitation of the stator teeth.

In a second step the mechanical structure-dynamic FE-model is presented. From the electromagnetic model the surface-force density on the stator teeth is taken as excitation for the mechanical model. The results of the mechanical simulation are discussed in general and explicitly taking the eccentric rotor movement into consideration. In general, eccentricity results in higher deformation of stator and housing of the IM. Furthermore, it can be stated, that static eccentricity shows the highest negative impact to the body-sound of the IM also depending on the location of the smallest air gap. This corresponds to measurements.

Applying the 2D-multi-slice technique for the electromagnetic model allows a fast and accurate analysis of the structure-dynamic behaviour of an electrical machine, i.e. an IM.

References

[1] H. Jordan, *Geräuscharme Elektromotoren*, Verlag W. Giradet, Essen, 1950.

[2] P. L. Timar, *Noise and Vibration of Electrical Machines*, Elsevier Science Publishing Company, New York, 1998.

[3] A. Tenhunen, T. P. Holopainen, A. Arkkio, "Effects of saturation on the forces in induction motors with whirling cage rotor," *IEEE Trans. on Magn.*, vol 40, no. 2, pp. 766 - 769, March 2004.

[4] J. Rusek, "Diagnostic oriented computer model of the induction machine, accounting for eccentricities and slotting," *2nd International Seminar on Vibrations and Acoustic Noise of Electric Machinery, VANEM*, pp. 75 - 79, September 2000.

[5] O. C. Zienkiewicz, R. L. Taylor, *„The finite element method,"* McGraw-Hill Book Company, London, 1989.

[6] A. Kost, *"Numerische Methoden in der Berechnung elektromagnetischer Felder,"* Springer-Verlag, Berlin, Heidelberg, New York, Barcelona, Budapest, Hon Kong, London, Mailand, Paris, Santa Clara, Singapore, Tokyo, 2000.

[7] H. De Gersem, J. Gyselinck, P. Dular, K. Hameyer, T. Weiland, „Comparison of sliding-surface and moving-band techniques in frequency-domain finite-element models of rotating machines," *COMPEL*, vol 23, no. 4, pp. 1006 – 1014, November 2004.

[8] C. Schlensok, G. Henneberger, "Comparison of static, dynamic, and static-dynamic eccentricity in induction machines with squirrel-cage rotors using 2D-transient FEM," *COMPEL*, vol 23, no. 4, pp. 1070 – 1079, November 2004.

[9] D. van Riesen, C. Monzel, C. Kaehler, C. Schlensok, G. Henneberger, "iMOOSE-an open-source environment for finite-element calculations," *IEEE Trans. on Magn.*, vol 40, no. 2, pp. 1390 - 1393, March 2004.

[10] J. P. A. Bastos, N. Sadowski, *Electromagnetic modelling by finite element methods*, Marcel Dekker, Inc., New York, Basel, 2003.

[11] J. J. C. Gyselinck, L. Vandevelde, J. A. A. Melkebeek, "Multi-slice FE modelling of electrical machines with skewed slots – the skew discretization error," *IEEE Trans. on Magn.*, vol 37, no. 5, pp. 3233 - 3237, September 2001.

[12] C. Schlensok, D. van Riesen, T. Küest, G. Henneberger, "Acoustic calculation of an induction machine with squirrel-cage rotor," *COMPEL*, vol. 25, no. 2, pp 475-486, April 2006.